Eur. Phys. J. A **23**, 217–222 (2005)
DOI 10.1140/epja/i2004-10092-x

THE EUROPEAN PHYSICAL JOURNAL A

The $i_{13/2}$ proton intruder orbital and the identical superdeformed bands in ^{193,194,195}Tl

X.T. He[1,2,a], S.X. Liu[1,3], S.Y. Yu[1,4], J.Y. Zeng[1,3], and E.G. Zhao[1,2,4]

[1] Center of Theoretical Physics, National Laboratory of Heavy Ion Accelerator, Lanzhou 730000, PRC
[2] Institute of Theoretical Physics, the Chinese Academy of Sciences, Beijing 100080, PRC
[3] School of Physics, Peking University, Beijing 100871, PRC
[4] College of Science, Huzhou University, Huzhou 313000, PRC

Received: 14 July 2004 / Revised version: 6 October 2004 /
Published online: 14 December 2004 –
Communicated by A. Molinari

Abstract. The microscopic mechanism of the identical bands in odd-odd nucleus ^{194}Tl and its neighbor odd-A nuclei ^{193,195}Tl is investigated using the particle-number–conserving (PNC) method for treating the cranked shell model with monopole and quadrupole pairing interactions. It is found that the blocking effect of the high-j intruder orbital plays an important role in the variation of moments of inertia ($J^{(1)}$ and $J^{(2)}$) with rotational frequency for the superdeformed bands and identical bands. The ω variation of the occupation probability of each cranked orbital and the contributions to moment of inertia from each cranked orbital are presented.

PACS. 21.60.Cs Shell model – 21.10.Re Collective levels – 27.80.+w $190 \leq A \leq 219$

1 Introduction

The first observation of superdeformation (SD) in the $A \sim 190$ mass region was reported [1] about ten years ago. Since then, more than 80 SD bands have been observed in this region (see ref. [2]). The superdeformation at high spin remains one of the most challenging topics of nuclear structure [3]. At present, although a general understanding of this phenomenon has been achieved, there are still many open problems. For the underlying physics of the superdeformed identical bands (IBs) (see the review [4]), some studies [5,6] showed that there is special physics or symmetry behind IBs, while others [7–9] suggested the same γ-ray transition energy and the identical moment of inertia (MoI) are due to the competition among the shell effect (stretching effect), pairing interaction, blocking effect, rotation alignment and Coriolis anti-pairing effect. Although a lot of theoretical work has been done based on various models (*e.g.*, particle-plus-core model, mean-field approximation, symmetry-based approach, etc.) which are successful for various aspects to study the superdeformed nuclei, they are still far from a precise quantitative description.

In the $A \sim 190$ region, for most SD bands in even-even and odd-A nuclei, the dynamical moment of inertia ($J^{(2)}$) exhibits a gradual increase with the increasing rotational frequency $\hbar\omega$, which is due to the gradual alignment of nucleons occupying high-N intruder orbitals (originating from the $i_{13/2}$ proton and $j_{15/2}$ neutron subshells) in the presence of the pair correlation, while in the odd-odd nuclei, quite a good part of the moments of inertia for SD bands keep constant. Experiments show that there do exist systematic odd-even differences in MoI at low spin, $J\,(\text{even-even}) < J\,(\text{odd-}A) < J\,(\text{odd-odd})$, which is the manifestation of blocking effect on pairing. IBs are observed both in odd-odd and even-even nuclei with their neighbor odd-A nuclei. For the abundant experimental data, many works on the SD bands and the identical bands have been done in even-even nuclei and their neighbor odd-A nuclei (see, *e.g.*, [7,8,10,11]). However, the SD bands and the identical bands in the odd-odd nuclei and their neighbor odd-A nuclei are seldom studied.

In this paper, the identical SD bands in the odd-odd nucleus ^{194}Tl and its neighbor odd-A nuclei ^{193,195}Tl are investigated by the particle-number–conserving (PNC) method [12,13] for treating the cranked shell model (CSM) with monopole and quadrupole pairing interactions, in which the particle number is conserved and the blocking effects are taken into account strictly. The PNC method has been used to study the normally deformed (ND) bands in the rare-earth nuclei at low spin, in which the observed systematics of the fluctuation in $\delta J/J$ for ND bands [14] and the set of identical ND bands [15] can be reproduced quite well and no free parameter is involved. A more

[a] e-mail: hext@itp.ac.cn

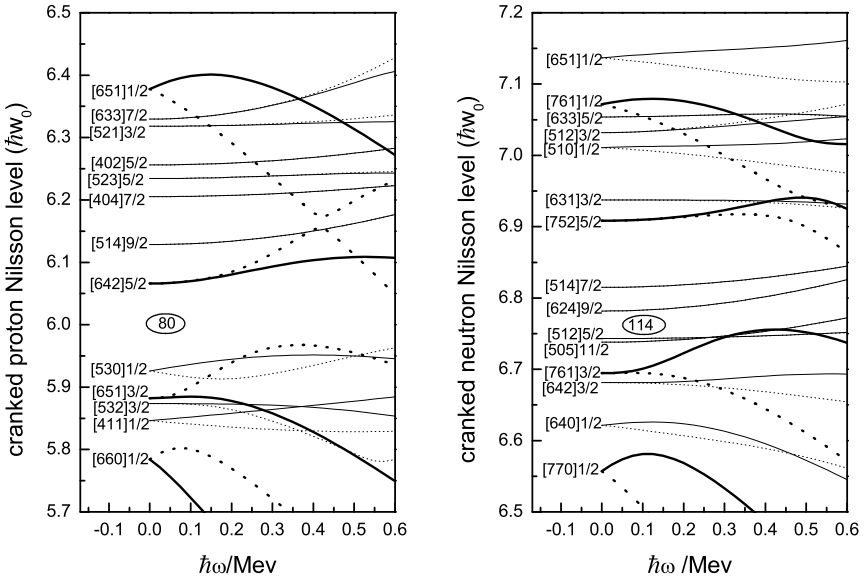

Fig. 1. The cranked proton and neutron Nilsson orbitals near the Fermi surface in the $A \sim 190$ region. The solid (dotted) line stands for $\alpha = +1/2$ ($\alpha = -1/2$), and the intruder high-N orbitals are denoted by the bold line.

detailed information on the separate contributions to MoI from each cranked orbital is also clearly exhibited. Recently, we have made a PNC calculation for the set of the identical SD bands in Hg isotopes and it works well [7].

In the next section, the formalism of the approach will be briefly sketched (see ref. [13] for details). In sect. 3, the calculated results and discussions are presented. Finally, conclusion and remarks are given in sect. 4.

2 Formalism

The CSM Hamiltonian with pairing interactions reads as

$$H_{\rm CSM} = H_{\rm SP} - \omega J_x + H_{\rm P} = H_0 + H_{\rm P}, \qquad (1)$$

where $H_0 = H_{\rm SP} - \omega J_x = \sum_i h_0(\omega)_i$, ($i$ includes all the valence particles), $h_0(\omega) = h_{\rm Nilsson} - \omega j_x$, is the one-body part of $H_{\rm CSM}$, $H_{\rm Nilsson}$ the Nilsson Hamiltonian, $-\omega j_x$ the Coriolis interaction and $H_{\rm P}$ the pairing interaction including both monopole and quadrupole pairing interactions: $H_{\rm P} = H_{\rm P}(0) + H_{\rm P}(2)$, where

$$\begin{aligned} H_{\rm P}(0) &= -G_0 \sum_{\xi\eta} a^\dagger_\xi a^\dagger_{\overline{\xi}}\, a_{\overline{\eta}}\, a_\eta \\ &= -G_0 \sum_{\xi\eta} (-)^{\Omega_\xi - \Omega_\eta}\, a^\dagger_\xi a^\dagger_{-\xi}\, a_{-\eta}\, a_\eta, \qquad (2) \end{aligned}$$

$$H_{\rm P}(2) = -G_2 \sum_{\xi\eta} q_2(\xi)\, q_2(\eta)\, a^\dagger_\xi\, a^\dagger_{\overline{\xi}}\, a_{\overline{\eta}}\, a_\eta \qquad (3)$$

with $\left|\overline{\xi}\,(\overline{\eta})\right\rangle$ being the time-reversal state of $|\xi\,(\eta)\rangle$ and $q_2(\xi) = \sqrt{16\pi/5}\,\langle\xi|\, r^2 Y_{20}\,|\xi\rangle$ the diagonal element of the stretched quadrupole operator. In our calculations, $h_0(\omega)$ is firstly diagonalized to obtain the cranked Nilsson orbitals. Then, $H_{\rm CSM}$ is diagonalized in a sufficiently large cranked many-particle configuration (CMPC) space to obtain the yrast and low-lying eigenstates.

The eigenstate of $H_{\rm CSM}$ is expressed as

$$|\psi\rangle = \sum_i C_i\,|i\rangle\,, \qquad (4)$$

where $|i\rangle$ denotes an occupation of particles in the cranked orbitals and C_i is the corresponding probability amplitude. The occupation probability of the cranked orbital μ (including both signatures $\alpha = \pm 1/2$) is

$$\begin{aligned} n_\mu &= \sum_i |C_i|^2 P_{i\mu}, \\ P_{i\mu} &= \begin{cases} 1, & |\mu\rangle \text{ is occupied in CMPC}|i\rangle, \\ 0, & \text{otherwise.} \end{cases} \end{aligned} \qquad (5)$$

The angular-momentum alignment is calculated as

$$\langle\psi|\, J_x\,|\psi\rangle = \sum_i |C_i|^2\,\langle i|\, J_x\,|i\rangle + 2\sum_{i<j} C_i^* C_j\,\langle i|\, J_x\,|j\rangle\,. \qquad (6)$$

Because J_x is a one-body operator, $\langle\psi|J_x|\psi\rangle (i \neq j)$ does not vanish only when $|i\rangle$ and $|j\rangle$ differ by one particle occupation. After a certain permutation of creation operators, $|i\rangle$ and $|j\rangle$ are expressed as

$$|i\rangle = (-)^{M_{i\mu}}|\mu\cdots\rangle, \qquad |j\rangle = (-)^{M_{j\nu}}|\nu\cdots\rangle, \qquad (7)$$

where the ellipsis stands for the same particle occupation and $(-)^{M_{i\mu}} = \pm 1, (-)^{M_{i\nu}} = \pm 1$ according to whether the permutation is even or odd. Then the dynamical moment of inertia of $|\psi\rangle$ is obtained:

$$J^{(2)} = {\rm d}\,\langle\psi|\, J_x\,|\psi\rangle\,/{\rm d}\omega = \sum_\mu j^{(2)}(\mu) + \sum_{\mu<\nu} j^{(2)}(\mu\nu), \quad (8)$$

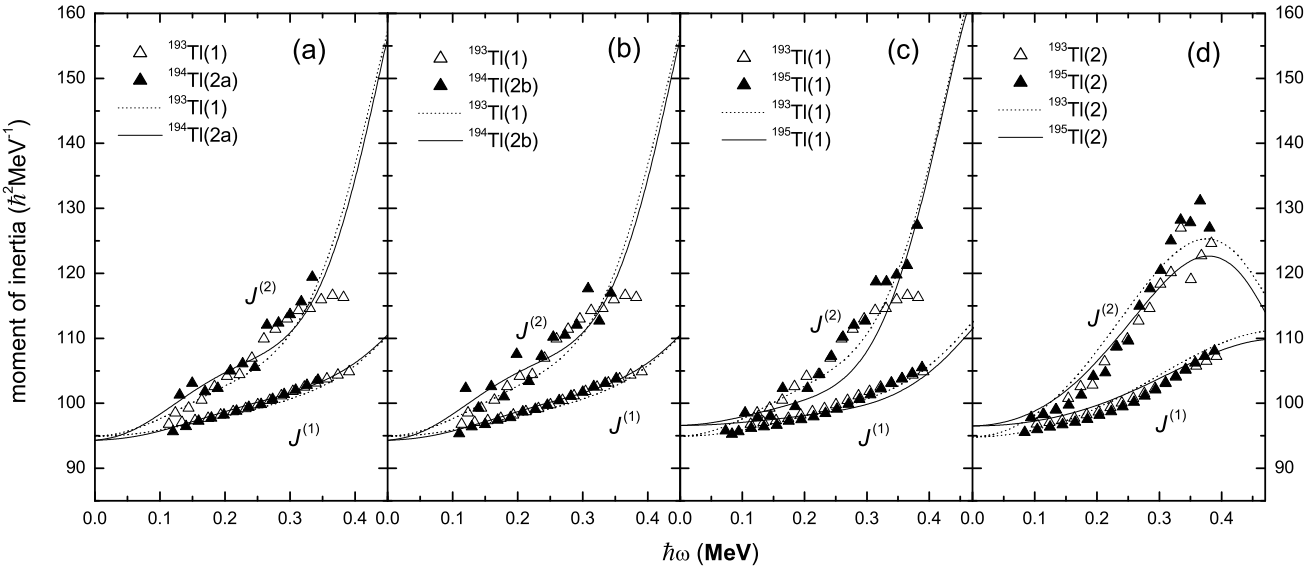

Fig. 2. Experimental and calculated $J^{(1)}$ and $J^{(2)}$ of the set of identical bands in ^{193,194,195}Tl.

where

$$j^{(2)}(\mu) = \frac{\mathrm{d}\,\langle\mu|\,j_x\,|\mu\rangle}{\mathrm{d}\omega} n_\mu,$$

$$j^{(2)}(\mu\nu) = 2\frac{\mathrm{d}\,\langle\mu|\,j_x\,|\nu\rangle}{\mathrm{d}\omega} \sum_{i<j} (-)^{M_{i\mu}+M_{j\nu}} C_i^* C_j \quad (\mu \neq \nu),$$

with $j^{(2)}(\mu)$ being the direct contribution to $J^{(2)}$ from a particle occupying the cranked orbital μ and $j^{(2)}(\mu\nu)$ being the contribution from the interference between two particles occupying the cranked orbital μ and ν which has no counterpart in the mean-field (BCS) treatment. We found that $j^{(2)}(\mu\nu)$ plays an important role for the odd-even difference and nonadditivity in MoI [16,17]. The expression for the kinematic moment of inertia $J^{(1)} = \langle\psi|\,J_x\,|\psi\rangle\,/\omega$ is similar to $J^{(2)}$ and can be found in [18].

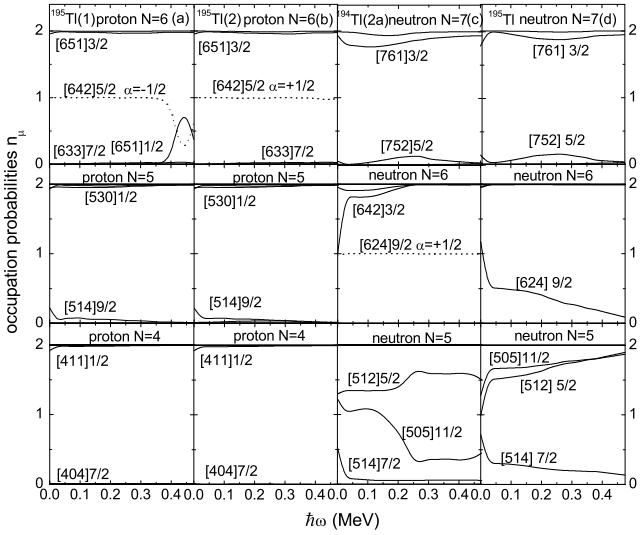

Fig. 3. Occupation probabilities n_μ of each proton and neutron cranked orbital μ near the Fermi surface. The blocked orbitals are denoted by the dotted line.

3 Calculated result and discussions

In our calculation, the spin assignments of these SD bands are taken from ref. [19], the Nilsson parameters (κ, μ) are taken from ref. [20] (for neutron $N = 6$ shell, their values are shifted slightly), the deformation parameters are $\varepsilon_2 = 0.46$ and $\varepsilon_4 = 0.03$. The cranked Nilsson orbitals near the Fermi surface for the SD bands in the $A \sim 190$ mass region are shown in fig. 1. For ND bands in the rare-earth nuclei, the pairing interaction strengths are determined by the experimental odd-even differences in binding energies and bandhead MoI. For SD bands in the $A \sim 190$ region, however, no experimental binding energies are available. The effective pairing strengths are determined by fitting the values of $J^{(1)}$ for ^{195}Tl(2) from $\hbar\omega \approx 0.10$–0.40 MeV. The effective pairing strengths also depend on the dimension of the truncated CMPC space. In the following calculation, the truncated CMPC's energy E_c is set about $0.65\hbar\omega_0$ (the corresponding CMPC's space dimensions are about 700) and $0.45\hbar\omega_0$ (the corresponding CMPC's space dimensions are about 1000) for proton and neutron, respectively, with $\hbar\omega_0 = 41A^{-1/3}$MeV. In such a CMPC space, the effective pairing interaction strengths (G_0 for monopole and G_2 for quadrupole pairing interaction) in unit of MeV are given as follows:

$$G_{0p} = 0.3, \quad G_{0n} = 0.2, \quad G_{2p} = 0.01, \quad G_{2n} = 0.013\,.$$

The experimental and calculated identical bands

$$\{^{193}\mathrm{Tl}(1),\, ^{194}\mathrm{Tl}(2\mathrm{a})\}, \quad \{^{193}\mathrm{Tl}(1),\, ^{194}\mathrm{Tl}(2\mathrm{b})\},$$
$$\{^{193}\mathrm{Tl}(1),\, ^{195}\mathrm{Tl}(1)\}, \quad \{^{193}\mathrm{Tl}(2),\, ^{195}\mathrm{Tl}(2)\}$$

are shown in fig. 2. For the experimental kinematic moment of inertia $J^{(1)}$, we can see that the four pairs of

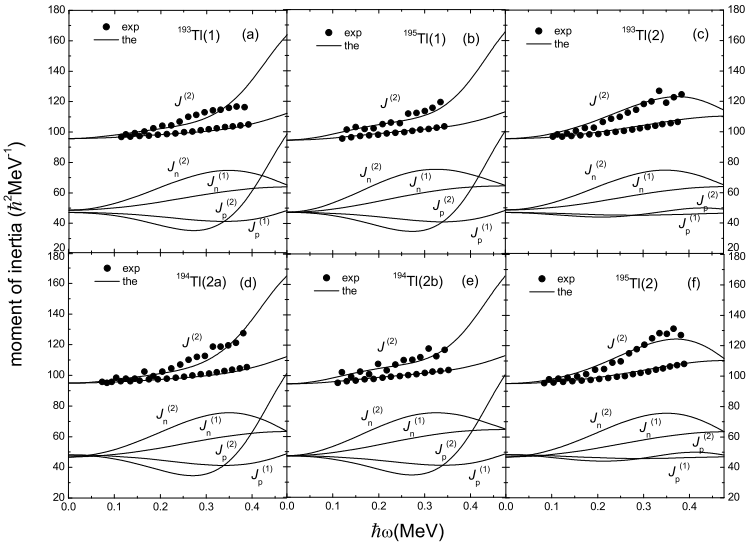

Fig. 4. The separate contributions to $J^{(1)}$ and $J^{(2)}$ from neutrons and protons ($J_n^{(1)}$ and $J_p^{(2)}$).

Table 1. The configurations of the six SD bands in ^{193,194,195}Tl.

SD band	Configuration
^{193}Tl$(1, \alpha = -1/2)$	$(\pi[642]5/2, \alpha = -1/2)$
^{193}Tl$(2, \alpha = +1/2)$	$(\pi[642]5/2, \alpha = +1/2)$
^{194}Tl$(2\mathrm{a}, \alpha = 0)$	$(\pi[642]5/2, \alpha = -1/2) \otimes (\nu[624]9/2, \alpha = +1/2)$
^{194}Tl$(2\mathrm{b}, \alpha = 1)$	$(\pi[642]5/2, \alpha = -1/2) \otimes (\nu[624]9/2, \alpha = -1/2)$
^{195}Tl$(1, \alpha = -1/2)$	$(\pi[642]5/2, \alpha = -1/2)$
^{195}Tl$(2, \alpha = +1/2)$	$(\pi[642]5/2, \alpha = +1/2)$

identical bands display "striking similarities" in the frequency range $0.10 < \hbar\omega < 0.35$ MeV for $\{^{193}\mathrm{Tl}(1), ^{194}\mathrm{Tl}(2\mathrm{a})\}$, $\{^{193}\mathrm{Tl}(1), ^{194}\mathrm{Tl}(2\mathrm{b})\}$, and $0.10 < \hbar\omega < 0.40$ MeV for $\{^{193}\mathrm{Tl}(1), ^{195}\mathrm{Tl}(1)\}$, $\{^{193}\mathrm{Tl}(2), ^{195}\mathrm{Tl}(2)\}$. The similarities of these bands are reproduced quite well in our calculations in the observed frequency range. For the dynamical moment of inertia $J^{(2)}$, a sharp increase in the experimental SD band of the ^{195}Tl(1) occurs at $\hbar\omega > 0.35$ MeV, while it is not obvious for ^{193}Tl(1). However, our calculated results show this abrupt uptrend both in ^{193}Tl(1) and ^{195}Tl(1) which we will explain later. For the first set of IBs, $\{^{193}\mathrm{Tl}(1), ^{194}\mathrm{Tl}(2\mathrm{a})\}$, $\{^{193}\mathrm{Tl}(1), ^{194}\mathrm{Tl}(2\mathrm{b})\}$ and $\{^{193}\mathrm{Tl}(1), ^{195}\mathrm{Tl}(1)\}$ (figs. 2(a), (b) and (c)), the blocked proton orbital is $[642]5/2\alpha = -1/2$ in the frequency range $0.10 < \hbar\omega < 0.35$MeV. For the second set of IBs, $\{^{193}\mathrm{Tl}(2), ^{195}\mathrm{Tl}(2)\}$ (fig. 2(d)), the blocked proton orbital is $[642]5/2\alpha = +1/2$ in the frequency range $0.10 < \hbar\omega < 0.4$ MeV.

The proton and neutron occupation probabilities n_μ of each cranked Nilsson orbital near the Fermi surface *versus* rotational frequency are given in fig. 3 (the orbitals with $n_\mu = 0$ or $n_\mu = 2$ are not shown here). The configurations (see table 1) of all the six bands agree with the assignments of the experimental studies [21,22].

As for the proton, the occupation probabilities in ^{194}Tl(2a,2b) and ^{193}Tl(1,2) are not shown here for the similarity with that in ^{195}Tl(1,2). As shown in fig. 3 ((a), (b)), the blocking of individual proton high-j intruder orbital [642]5/2 is obvious. It is known that the blocking effect is very important when the high-j orbital near the Fermi surface is blocked. While the $[642]5/2(\alpha = -1/2)$ orbital is blocked in ^{195}Tl(1), another high-j orbital $[651]1/2(\alpha = -1/2)$ goes down with increased frequency and gets very close to the Fermi surface at $\hbar\omega \sim 0.38$ MeV (see fig. 1). Thus, at $\hbar\omega > 0.35$ MeV, there is an exchange of the occupation between $[642]5/2(\alpha = -1/2)$ and $[651]1/2(\alpha = -1/2)$ orbitals in ^{195}Tl(1), while $[642]5/2(\alpha = +1/2)$ still keeps fully occupied in ^{195}Tl(2). The calculated sharp increases of $J^{(2)}$'s for ^{193}Tl(1), ^{194}Tl(2a,2b) and ^{195}Tl(1) occurring at $\hbar\omega > 0.35$ MeV are due to the large contributions from the high-j intruder orbital $[651]1/2(\alpha = -1/2)$. This is the reason why a sharp increase occurs in ^{195}Tl(1) but a downturn occurs in ^{195}Tl(2). It is also the case occurring in ^{193}Tl(1) and ^{193}Tl(2). In experiment, there is no obvious uptrend occurring in ^{193}Tl(1). Considering the same configurations of the ^{193}Tl(1) and ^{195}Tl(1) and the explanations given above, we would like to persist in our conclusion. Our results will be tested by the farther experimental data extended to the higher frequency range.

As for the neutron, there are no blocked neutron orbitals in ^{193}Tl and ^{195}Tl. The occupation probabilities in ^{193}Tl are not shown here since they are similar to that in ^{195}Tl, except that the exceeded two neutrons in ^{195}Tl partially occupied the [512]5/2 orbital (see fig. 3(d)). For the same reason, we just display the occupation probabilities in ^{194}Tl(2a) (fig. 3(c)). The blocking effect is exhibited clearly by the neutron occupation probabilities. The blocked orbital is the high-Ω orbital ($[624]9/2(\alpha = +1/2)$) in ^{194}Tl(2a) and the corresponding Coriolis response is very small. Thus the occupation probabilities of this orbital keep constant ($n_\mu = 1$) up to rather high $\hbar\omega$ and the contributions to the moment of inertia coming from the blocked orbital $[624]9/2(\alpha = \pm 1/2)$ in ^{194}Tl(2a) are negligible. From this one can understand why there are identical moments of inertia in ^{194}Tl(2a) and ^{193}Tl(1).

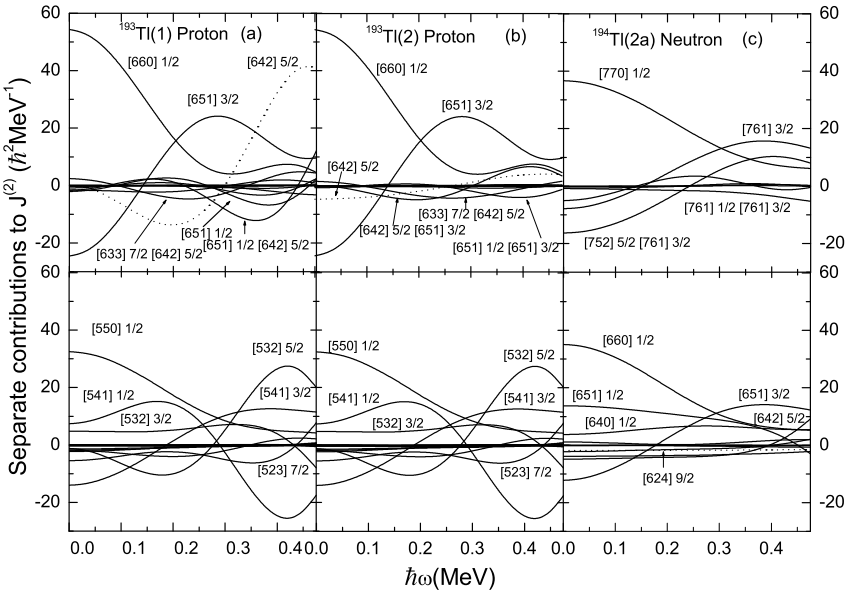

Fig. 5. The calculated contributions to $J^{(2)}$ from each cranked proton and neutron orbital near the Fermi surface, $j^{(2)}(\mu)$ (the line indicated by one orbital) and $j^{(2)}(\mu\nu)$ (the line indicated by two orbitals). The contributions to $J^{(2)}$ from the blocked orbitals are denoted by the dotted line.

It is noted that the frequency range for the set of identical bands in Hg isotopes ($\hbar\omega > 0.2$ MeV) is higher than that in Tl isotopes ($\hbar\omega > 0.1$ MeV). The underlying physics is that the blocking effect on MoI is sensitive to the Coriolis response of the blocked orbitals. For the set of IBs in Tl isotopes, the blocked proton orbitals are the same high-j orbital [642]5/2. The blocked neutron orbitals in ^{194}Tl(2a,2b) are the high-Ω orbitals [624]9/2, whose Coriolis response is very small. So the pair of IBs in Tl is identical in almost the whole observed frequency. For Hg isotopes, IBs are between the yrast band and the excited bands based on high-Ω orbitals and the values of band-head MoI J_0 are not identical due to the blocking effect.

The separate contributions to $J^{(1)}$ and $J^{(2)}$ from neutrons and protons are shown in fig. 4. It is seen that the contributions from neutrons for all the six bands are similar no matter whether there are the blocked orbitals or not. This is because the blocked orbital in ^{194}Tl(2a,2b) is the high-Ω orbital ([624]9/2($\alpha = \pm 1/2$)), the corresponding Coriolis response is very small and the contributions to the moment of inertia from the blocked orbital [624]9/2($\alpha = \pm 1/2$) in ^{194}Tl(2a,2b) are negligible. The contributions from protons are larger than neighboring even-even nuclei SD bands because of the blocking effect of the single proton intruder orbital [642]5/2 (see fig. 1), which is affected significantly by the Coriolis interaction. It is obvious that all the six bands can be classified as two categories, two set of IBs ($\{^{193}$Tl(1),^{194}Tl(2a),^{194}Tl(2b),^{195}Tl(1)$\}$ and $\{^{193}$Tl(2),^{195}Tl(2)$\}$) according to the odd proton occupying [624]9/2($\alpha = +1/2$) or [624]9/2($\alpha = -1/2$). From this we can see that the blocked proton high-j orbital plays an important role in the ω variation of MoI. We take ^{195}Tl(1) and ^{195}Tl(2) (fig. 4(b), (e)) as an example to illustrate it. At $\hbar\omega < 0.3$ MeV, the increase of $J^{(2)}$ mainly comes from neutron's contributions while the proton's contributions increase at $\hbar\omega > 0.3$ MeV and become dominant at $\hbar\omega > 0.4$ MeV because of the large contributions coming from the high-j intruder orbital [651]1/2($\alpha = -1/2$). But for ^{195}Tl(2), there are neither the bands across nor the sharp increase of the $J_p^{(2)}$ contributions.

Our PNC calculations can provide more detailed information on the separate contributions to MoI from each cranked orbital (see fig. 5), which include the direct contributions $j^{(2)}(\mu)$ from orbital μ and the interference terms $j^{(2)}(\mu\nu)$ between orbitals μ and ν (see eq. (8)). It is well known that a closed major shell has no contributions to MoI. For SD bands in the $A \sim 190$ region, neutron $N \leq 4$ and proton $N \leq 3$ shells are closed. Neutron $N = 5$ and proton $N = 4$ shells are not shown here for the small constant contributions. We just display the proton contributions of ^{193}Tl(1,2) (fig. 5(a), (b)) and neutron contributions of ^{194}Tl(2a) (fig. 5(c)). As for the others, there are almost same neutron contributions among ^{193}Tl, ^{194}Tl(2a,2b) and ^{195}Tl, and similar proton contributions among ^{193}Tl(1), ^{194}Tl(2a,2b) and ^{195}Tl(1), ^{193}Tl(2) and ^{195}Tl(2).

It is noted that the contributions to MoI from each cranked orbital are sensitive to the location and in particular to the Coriolis response of the orbitals μ and ν. The orbitals far above or below the Fermi surface contribute little to MoI. In contrast, the blocking of intruder orbitals near the Fermi surface will strongly influence the MoI. For ^{193}Tl(1) and ^{195}Tl(1), at $\hbar\omega > 0.35$ MeV, the sharp increase of the $J^{(2)}$ mainly comes from the direct contributions $j^{(2)}(\mu)$ of the high-j intruder orbitals [642]5/2 and [651]1/2 and their interference terms $j^{(2)}([651]1/2[642]5/2)$, $j^{(2)}([642]5/2[633]7/2)$. As for ^{193}Tl(2) and ^{195}Tl(2), there is no band crossing occurring at $\hbar\omega > 0.35$ MeV, the contributions from the high-j

intruder orbitals [642]5/2 and [651]1/2 and their interference terms $j^{(2)}(\mu\nu)$ are small so there is no such a sharp increase. The contributions to $J^{(2)}$ from the high-Ω orbital is small and negligible while that from the high-j orbital is important. For example, we look at the point $\hbar\omega = 0.15$ MeV, where two bands in ^{194}Tl(2a) have very pure configurations (see fig. 3(c)) according to the experimental data and our calculation. The contribution coming from blocked neutron orbital [624]9/2 is $-1.7744\hbar^2$ MeV^{-1} and from their interference term $j^{(2)}([624]9/2[633]7/2)$ is $-0.0689\hbar^2$ MeV^{-1} while that coming from the blocked proton orbital [642]5/2 is $-12.1504\hbar^2$ MeV^{-1} and the interference term $j^{(2)}([642]5/2[651]1/2)$ is $2.4544\hbar^2$ MeV^{-1}.

4 Summary

In summary, the PNC method for treating the cranked shell model with monopole and quadrupole pairing interactions has been used to investigate the microscopic mechanism of the identical SD bands in the typical odd-odd nucleus ^{194}Tl and their neighbor odd-A nuclei ^{193,195}Tl. It is found that the blocking effect is very important and its influence on MoI depends on the orbital location and the Coriolis response of the blocked levels. The blocked proton orbital [642]5/2($\alpha = \pm 1/2$) plays a very important role in IBs, while the blocked neutron orbital [624]9/2($\alpha = \pm 1/2$) contributes little to the MoI. The contribution from the interference term ($j^{(2)}(\mu\nu)$), which has no counterpart in the mean-field (BCS) treatment, is very important and cannot be negligible.

This work was supported by National Natural Science Foundation of China under Grant Nos. 10375001 and 10147205, the Major State Basic Research Development Program under Grant No. G2000-0774-07 and the Knowledge Innovation Project of the Chinese Academy of Sciences under Grant No. KJCX2-SW-N02.

References

1. E.F. Moore *et al.*, Phys. Rev. Lett. **63**, 360 (1989).
2. Balraj Singh, Roy Zywina, Richard B. Firestone, Nucl. Data Sheets **97**, 241 (2002).
3. A.V. Afanasjev, P. Ring, J. König, Nucl. Phys A **676**, 196 (2000).
4. C. Baktash, B. Hass, W. Nazarewicz, Annu. Rev. Nucl. Part. Sci. **45**, 485 (1995) and references therein.
5. Z. Szymanski, W. Nazarewicz, Phys. Lett. B **433**, 229 (1998).
6. Y.X. Liu *et al.*, Phys. Rev. C **59**, 2511 (1999); **63**, 054314 (2001).
7. S.X. Liu, J.Y. Zeng, E.G. Zhao, Phys. Rev. C **66**, 024320 (2002).
8. Y. Sun, J.Y. Zhang, M. Guidry, Phys. Rev. Lett. **78**, 2321 (1997); Phys. Rev. C **63**, 047306 (2001).
9. Lennart B. Karlsson, Ingemar Kagnarsson, Sven Åberg, Phys. Lett. B **416**, 16 (1998).
10. J. Terasaki *et al.*, Phys. Rev. C **55**, 1231 (1997).
11. S. Kuyucak, M. Honma, T. Otsuka, Phys. Rev. C **53**, 2194 (1996).
12. X.B. Xin *et al.*, Phys. Rev. C **62**, 067303 (2000).
13. J.Y. Zeng *et al.*, Phys. Rev. C **50**, 1388 (1994).
14. J.Y. Zeng, Y.A. Lei, T.H. Jin, Z.J. Zhao, Phys. Rev. C **50**, 746 (1994).
15. J.Y. Zeng, S.X. Liu, Y.A. Lei, L. Yu, Phys. Rev. C **63**, 024305 (2001).
16. S.X. Liu, J.Y. Zeng, L. Yu, Nucl. Phys. A **735**, 77 (2004).
17. S.X. Liu, J.Y. Zeng, Nucl. Phys. A **736**, 269 (2004).
18. J.Y. Zeng *et al.*, Phys. Rev. C **65**, 044307 (2002).
19. S.X. Liu, J.Y. Zeng, Phys. Rev. C **58**, 3266 (1998).
20. T. Bengtsson, I. Ragnarsson, Nucl. Phys. A **436**, 14 (1985).
21. S. Bouneau *et al.*, Phys. Rev. C **53**, R9 (1996).
22. J. Duprat *et al.*, Phys. Lett. B **341**, 6 (1994).